uc3m | Universidad Carlos III de Madrid

e-Archivo

This is a postprint/accepted version of the following published document:

Puertas, F.; Torres, M., et al. Use of glass waste as an activator in the preparation of alkali-activated slag. Mechanical strength and paste characterisation, In: *Cement and Concrete Research, Vol.* 57, *March 2014, Pages 95-104*

DOI: https://doi.org/10.1016/j.cemconres.2013.12.005

© 2013 Elsevier Ltd. All rights reserved.

This work is licensed under a Creative Commons Attribution-NonCommercial-NoDerivatives 4.0 International License.

Use of glass waste as an activator in the preparation of alkali-activated slag. Mechanical strength and paste characterisation

F. Puertas* and M. Torres

Eduardo Torroja Institute for Construction Science (IETcc-CSIC), 28033 Madrid, Spain
*Corresponding author: e-mail address: puertasf@ietcc.csic.es

Abstract

The alkaline activation of aluminosilicates yields alkaline cements, eco-efficient alternatives to ordinary Portland cements. Alkaline cements and concretes exhibit highest strength and longest durability when activated with a solution of alkaline silicate hydrates (waterglass). To obtain these alkaline silicates, however, an aqueous solution of the proper proportion of carbonate and silica salts must be heated to temperatures of around 1 300 °C. The present paper explores the feasibility of using urban and industrial glass waste as a potential alkaline activator for blast furnace slag (AAS).

AAS pastes were prepared with three activators: waterglass, a $NaOH/Na_2CO_3$ mix and the solutions resulting from dissolving glass waste in $NaOH/Na_2CO_3$. Mechanical, mineralogical (XRD, FTIR) and microstructural (porosimetry, NMR and SEM/EDX) trials were conducted to characterise the pastes obtained.

The findings proved the feasibility of using glass waste to alkali activate slag. Treating glass waste with $NaOH/Na_2CO_3$ (pH=13.6) favours the partial dissolution of the Si in the glass into its most reactive monomeric form.

The solutions resulting from the treatment of glass waste act as alkaline activators, partially dissolving vitreous blast furnace slag. The composition and microstructure of the reaction products identified in the two types of paste were similar. Strength and microstructural development in the pastes activated with glass waste were also comparable to the parameters observed in AAS pastes prepared with conventional activators.

Keywords: Alkali-activated slag, glass waste, mechanical strength, characterisation, alternative alkaline activators

1. Introduction

Portland cement production is characterised by high energy demands, the consumption of non-renewable prime materials and the emission of greenhouse gases (essentially CO_2) [1, 2]. In 1987, the term "sustainable development" was coined to mean the balance between technological development and conservation of the environment. Ever since, in pursuit of such a balance, the cement industry has been seeking ways to minimise the adverse side effects of its activity.

Alkali-activated materials constitute a possible alternative to Portland cement. A.O. Purdon [3], V. Glukhovsky [4, 5] and J. Davidovits [6] pioneered research in this area and developed the earliest alkaline cements. Interest in these materials blossomed in the rest of the world beginning in the nineteen nineties [7-21].

Alkaline activation calls for two basic components: preferably amorphous or vitreous aluminosilicates and an alkaline activator. The aluminosilicates may be natural products such as metakaolin or industrial by-products such as blast furnace slag or aluminosiliceous fly ash [17].

The alkaline solutions able to interact with aluminosilicates to generate such new binders include: alkaline metal or alkaline-earth hydroxides (ROH, $R(OH)_2$), weak acid salts (R_2CO_3, R_2S, RF), strong acid salts (Na_2SO_4, $CaSO_4 \cdot 2H_2O$) and $R_2O(n)SiO_2$-type siliceous salts, where R is an alkaline ion such as N, K or Li. From the standpoint of end product strength and other properties, the most effective of these activators are NaOH, Na_2CO_3 and sodium silicate hydrates [22, 23]. And of these, the solutions that induce the best mechanical behaviour in alkali-activated materials are waterglass-based [12, 24, 25].

The cements obtained by alkali-activating aluminosilicates are characterised by high mechanical strength [5], low heat of hydration [6] and high impermeability [27], as well as resistance to high and low temperatures [28, 29] and sulfate, sea spray and acid attack [27, 30-32].

A number of materials, including silica fume, pozzolans, rice husk ash [33] and others can be used as a supplementary source of silica in alkali-activated systems. Certain types of waste or industrial by-products can also be valorised to minimise the adverse (energy demand and CO_2 emissions) effect of the industrial production of sodium silicate, also known as waterglass,

which calls for heating an aqueous solution of the proper proportion of carbonate and silica salts calls to around 1 300 °C [34, 35].

The present study aimed to evaluate the feasibility of using glass waste as a source of silica to replace waterglass in the alkaline activation of blast furnace slag. Urban glass waste is an amorphous material with a chemical composition based essentially on SiO_2 (65-75 %), CaO (6-12 %), Na_2O (12-15 %), Al_2O_3 (0.5-5%) and Fe_2O_3 (0.1-3 %) [36-38].

One of the most prominent properties of glass, in addition to its transparency, is its high resistance to chemical attack. That notwithstanding, some interaction always takes place between glass and chemical substances. Glass is attacked by both acid and alkaline solutions, although the mechanisms and degree of corrosion differ [39]. Glass is highly soluble at alkaline pH values [40-42]. At values of 9 to 10.7, the solubility of amorphous silica rises due to the formation of silicate ions, along with a monomer in equilibrium with the solid phase. At values higher than 10.7, the amorphous silica in the solid phase dissolves to form a soluble silicate. High temperatures also favour glass solubility [42, 43].

Prior studies determined the solubility of different types of glass waste in highly alkaline media [35-37]. This waste has been found to dissolve most effectively (highest amounts of dissolved SiO_2 and Al_2O_3) when a 50/50 Molar solution of $NaOH/Na_2CO_3$ is heated at 80 °C for 6 h [44]. The question that must now be addressed is whether the solutions resulting from the treatment of glass waste can replace traditional waterglass in the preparation of alkaline cements. Consequently, the primary objective of the present research was to explore the feasibility of using urban and industrial glass waste as a potential alkaline activator for blast furnace slag.

2. Experimental

2.1. Materials

Table 1 gives the chemical composition of the Spanish vitreous blast furnace slag and the glass waste used in this study. The vitreous phase accounted for 99 % of the slag content (modified McMaster method) [45] and specific surface of this material was 325 m^2/kg (EN 196-6). XRD and FTIR characterisation confirmed the amorphous nature of both types of waste.

Table 1. Chemical composition of slag and glass (wt %)

The following activating solutions, all at a constant 5 % Na_2O by slag mass, were used:

- 50-per cent mix of NaOH and Na_2CO_3 in molar (Panreac analytical grade 98 % sodium hydroxide and 99.8 % sodium carbonate), yielding a solution with a pH of 13.6.
- commercial waterglass (Merck, 27 % SiO_2; 8 % Na_2O and 65 % H_2O by weight) with a SiO_2/Na_2O ratio of 1.2.
- 50-per cent (wt) $NaOH/Na_2CO_3$ solutions with different amounts of dissolved glass waste (from 1 to 25 grams per 100 mL of solution).

The last group was prepared by adding 1, 10, 15, 20 and 25 g of glass waste (with a particle size of under 45 μm) to the sodium hydroxide/sodium carbonate solution, stirring at 80 ± 2 °C for 6 h and subsequent filtering, as described in [34]. The ions dissolved in the filtered solutions were analysed by ICP-AES on a VARIAN 725-ES inductively coupled plasma atomic emission spectrometer. **Table 2** lists the weight of oxides dissolving out of the glass and into the activating solution (g/100 mL).

Table 2. SiO_2, Al_2O_3, CaO and MgO (g) from the glass waste dissolved after treatment in 100 ml of 50-per cent (wt) NaOH / Na_2CO_3

2.2 Paste preparation and trials conducted

Paste specimens measuring 1x1x6 cm were prepared to the compositions given in **Table 3**. The liquid/solid ratio was 0.4 or 0.44, depending on the type of activator, to ensure that plasticity was as recommended in European standard EN 196-3 in all cases. The pastes were chamber-cured (99 % relative humidity, 20 ± 2 °C) for 1, 2, 7 or 28 days and the prismatic specimens tested for mechanical strength.

The total porosity and pore size distribution were determined on pastes AAS N/C-25, AAS N/C and AAS WG at all ages. All other characterisation trials were conducted on the same pastes, but only on the 7-day specimens. After the mechanical tests, the pastes were immersed in acetone/ethanol to detain the hydration/activation process. The tests conducted on these pastes were Hg intrusion porosimetry, FTIR, XRD, ^{29}Si and ^{27}Al MAS NMR and BSEM/EDX.

Table 3. Pastes prepared and activation conditions

Mechanical strength tests were conducted on an Ibertest Autotest 200/10 hydraulic press as specified in European standard EN 196-1 at a rate of 2 400 N/s ± 200 N/s to failure. Total porosity and pore size distribution were found with Hg intrusion porosimetry on a

Micromeretics Autopore IV 9500 analyser able to exert pressure of up to 32 000 Psi (≈220 608 MPa, equivalent to a pore size as small as 0.0067 µm). The FTIR spectra were obtained by analysing KBr pellets containing 1.0 mg of sample in 300 mg of KBr on an ATIMATTSON Genesis Series FTIR-TM spectrometer. The spectra were recorded after running 64 scans in the 4 000-400 cm^{-1} range. The XRD patterns for the samples were recorded on a Bruker AXS D8 Advance diffractometer fitted with a Lynxeye super speed RX detector, a 2.2-kW Cu anode and no monochromator. The scanning range, from 5 to 60°, was covered in a 24-minutes period. The instrument was set at 40 kW and 30 mA and the sample was not rotated during scanning. The ^{29}Si and ^{27}Al solid state nuclear magnetic resonance (MAS NMR) spectra were obtained with a Bruker MSL 400 spectrometer operating at 79.49 and 104.26 MHz. All the spectra were packed into a 4-mm zirconium MAS rotor and spun at 10 000 Hz. For the ^{27}Al spectra, the relaxation time applied was 5 seconds and 360 acquisitions were obtained per scan. For the ^{29}Si spectra, the values were 10 seconds and 1 200 acquisitions. After the spectra were recorded, the curves were deconvoluted with dmfit software, which fits the theoretical to the experimental curves. The 7-day samples were embedded in an epoxy resin and subsequently cut, polished and carbon-coated for back-scattered electron microscopic examination on a JOEL JSM 5400 scanning electron microscope fitted with a solid state back-scattered detector. Microanalyses were conducted using LINK-ISIS energy dispersive X-ray (EDX) techniques.

3. Results

3.1 Mechanical strentgh and porosity

The mechanical performance of the pastes studied is reflected in **Figure 1**. The figure shows that compressive strength rose with curing time in all the pastes. The lowest strength values were recorded, at all ages, for paste AAS N/C, i.e., the paste prepared with $NaOH/Na_2CO_3$ as the activator, and the highest for paste AAS WG, prepared with waterglass.

The graph also shows that the higher the glass waste content in the activating solution in the AAS N/C family of pastes, the higher was their mechanical strength, although none was as strong as paste AAS WG.

Figure 1. Compressive strength of AAS pastes prepared with different alkaline activators

The total porosity and pore size distribution (in the 100-0.01 µm range) for the pastes are respectively given in **Figure 2**, where the porosity values are shown in percentage of the total sample volume.

According to the table, total porosity was greatest in paste AAS N/C at all ages, ranging from 18 to 24 %. In the pastes prepared with Si-containing activators, total porosity was significantly lower: 4-9 % in AAS WG and 7-9 % in paste AAS N/C-25.

Pore size distribution followed a similar pattern (**Figure 2**), with a greater proportion of micro- and mesopores in the pastes prepared with the activators containing silicon. The paste prepared with 25 g/100 mL glass waste had a larger fraction of pores smaller than 0.01 µm. These total porosity and pore size distribution findings are consistent with the compressive strength found for the materials tested (**Figure 1**).

Figure 2. Pore size distribution in pastes AAS N/C, AAS WG and AAS N/C-25

3.2 Characterization of reaction products

The FTIR spectra for the anhydrous slag and the 7-day alkali-activated pastes are shown in **Figure 3**. An analysis of these spectra confirmed that reaction products formed as a result of the alkaline activation of the slag. The FTIR spectra for the pastes showed that the Si-O vibration band generated by the SiO_4 groups in the anhydrous slag shifted from 996 cm^{-1} to 961-969 cm^{-1} due to the formation of a calcium aluminosilicate hydrate, a C-A-S-H-type gel [46-48]. The band at around 460 cm^{-1} was attributed to v_4 [Si-O-Si] bond vibrations, while the signal at around 669 cm^{-1} was due to the stretching vibrations generated by the Al-O bonds in the AlO_4 groups. The band at 1625 cm^{-1} was the result of the bending vibrations generated by the OH groups in the water. The spectra also contained signals at 1420 cm^{-1} attributed to $v_3[CO_3^{2-}]$, while the vibration bands detected between 875 and 711 cm^{-1} were associated with $v_2[CO_3^{2-}]$ and $v_4[CO_3^{2-}]$, respectively, confirming paste carbonation or weathering.

The bands in IR spectra for pastes AAS WG and AAS N/C-25, especially for the Al-O and Si-O vibrations, exhibited similar positions, widths and intensities. The 1300-1500 cm^{-1} range on the IR spectrum for AAS N/C-25 contained absorptions characteristic of carbonate groups, which were also identified on the IR spectrum for paste AAS N/C. These bands were attributed to the presence of calcium and calcium-sodium carbonates in the samples [49].

That finding was confirmed by XRD (see **Figure 3**), along with the formation of a C-S-H-type gel (JCPDS 34-0002) and the formation of calcium carbonates (JCPDS 24-27) according to the

reflection lines visible on the diffractograms for all the samples. The hydrotalcite ($Mg_6Al_2(CO_3(OH))_{16}{\cdot}4H_2O$) (JCPDS 22-0700) phase was also identified on the XRD patterns for all the pastes at $2\theta = 11.27°$ [50]. These XRD findings afforded further proof of the similarity between pastes AAS WG and AAS N/C-25.

Figure 3. FTIR spectra for the anhydrous slag and 7-day pastes; b) XRD patterns for the anhydrous slag and 7-day pastes

Figure 4 shows the ^{29}Si and ^{27}Al MAS NMR spectra for the anhydrous slag and the three 7-day AAS pastes. The identification of the components on the ^{29}Si NMR spectra was based on prior aluminosilicate studies [51-54]. The spectrum deconvolution data are listed in **Table 4**.

The ^{29}Si NMR spectrum for the anhydrous slag exhibited a wide signal at around -75.50 ppm. According to Richardson and Groves [55], that signal is associated with Q^0 units around -69 ppm, and to Schilling et al. [56], to Q^1 units around -73 ppm. Attributing the signal to Q^1 units would be a sign that the silicate groups present in the slag were organised primarily as dimers. The ^{27}Al MAS NMR spectrum for the anhydrous slag, in turn, had a signal centred on +59.38 ppm, associated with the presence of tetrahedrally coordinated aluminium (Al_T = 65.33 %). Two smaller signals at around +33.00 and +10.50 ppm, were respectively attributed to pentahedrally (Al_P = 23.19 %) and octahedrally (Al_O = 10.98 %) coordinated Al [47].

Table 4. Deconvolution data for ^{29}Si and ^{27}Al MAS NMR spectra by the nature of the activator (anhydrous slag and 7-day pastes)

The ^{29}Si MAS NMR spectrum for paste AAS N/C contained a wide signal with several peaks (**Figure 4a**). Its deconvolution revealed the presence of unreacted Q^0 and Q^1 units from the anhydrous slag. In addition, other signals were detected and attributed to Q^1 (end of chain), Q^2 (1Al), (0Al), Q^3 (1Al) and Q^3(0Al) units [46, 57]. These units were associated with the formation of C-A-S-H gel, the man reaction product in slag alkali-activation [46, 47]. The same signals were visible on the ^{29}Si MAS NMR spectrum for paste AAS WG, although clearly shifted toward more negative values. Lastly, the shape and deconvolution data for the paste AAS N/C-25 ^{29}Si MAS NMR spectrum were intermediate to the characteristics of the other two pastes.

The ^{27}Al MAS NMR spectra for anhydrous slag and the three pastes (**Figure 4b**) exhibited three clearly identified signals. Two were located in a wide, intense and asymmetrical band at

around 60 ppm: one centred on around 59 ppm and associated with tetrahedral aluminium (Al_T) and a smaller signal at around 31 ppm due to the presence of pentahedral aluminium (Al_P). A third, less intense but narrower signal, indicating the presence of octahedral aluminium (Al_o), appeared at 8 ppm [46, 57, 60]. The Al_T signal at 59 ppm was narrower on the spectra for the AAS WG and AAS N/C-25 pastes than on paste AAS N/C. That, together with the greater intensity of the signal, was an indication that part of the Al_T had been taken up into the structure of the C-A-S-H gel.

Figure 4. a) ^{29}Si and b) ^{27}Al MAS NMR spectra for the anhydrous slag and the 7-day alkali-activated pastes

The BSEM/EDX study conducted (see **Figure 5**) revealed microstructural differences in the pastes depending on the activator used in their preparation. Further to its micrograph, paste AAS N/C contained substantial quantities of anhydrous slag particles (see **Figure 5a**), as well as an open and scantly compact structure. Less anhydrous slag and a more compact and uniform C-A-S-H gel were observed in the paste AAS WG micrograph (see **Figure 5b**). The microcracks characteristic of the intense drying shrinkage associated with these pastes were likewise visible [65]. The AAS N/C-25 microstructure (**Figure 5c**) exhibited intermediate features, with smaller amounts of anhydrous slag than paste AAS N/C but a less uniform morphology than AAS WG. **Table 5** gives the results of local analyses in different zones of the C-A-S-H gel to determine their Ca/Si ratios, which were found to be around 1 or less.

Table 5. EDX determination of atomic radio

Figure 5. BSEM/EDX images of N/C-, WG- and N/C-25-activated slag pastes

4. Discussion

The analytical findings showed that silicon from glass waste dissolved in $NaOH/Na_2CO_3$ solutions can induce much the same effect as the silicon in waterglass.

As shown in **Table 2**, which gives glass waste solubility in 100 mL of $NaOH/Na_2CO_3$, the higher the glass content in the medium, the larger was the amount of dissolved silicon. **Figure 6**, in turn, reproduces the ^{29}Si MAS NMR spectrum for the original glass and the spectrum for the liquid obtained after treating the waste (1 g in 100 mL of alkaline solution) at 80 ± 2 °C for 2, 4 or 6 hours. The spectrum for the glass waste contained a single signal at around -93 ppm, indicative of the presence of the Q^4 Si units that characterise silica glass. The spectrum for the

post-treatment liquid, even at short times, exhibited a single signal at around -71 ppm, associated with the presence of Q^0 units, i.e., dissolved Si monomers. According to the literature [54, 66, 67], the effectiveness of Si in waterglass systems rises with declining condensation and polymerisation of the molecule in the medium.

These findings indicated that when glass waste was treated with a $NaOH/Na_2CO_3$ solution, part of its silicon dissolved into monomeric units, the form best suited for interacting with aluminosilicates liable to be alkali-activated.

The strength values found for paste AAS N/C-25 were observed to lie in between the strength developed by pastes AAS NC and AAS WG, although closer to the latter. The 28-day compressive strength in paste AAS N/C was 44 MPa, in paste AAS WG, 83 MPa and in paste AAS N/C-25, 66 MPa. That behaviour is consistent with the known facts that the nature of the alkaline activator is a determinant in alkali-activated slag pastes, mortars and concretes [23, 24, 61], and that waterglass-activated materials develop the highest strength. Another determinant in the strength of these materials is the SiO_2/Na_2O ratio in the waterglass solution, whose optimal value stands at around 1.0-1.5 [62]. According to the solubility data recorded (see **Table 2**), treating 25 g of glass waste in a $NaOH/Na_2CO_3$ solution yielded a solubility of 4.53 g/100 mL, from which the silica ratio in the solution used to prepare paste AAS N/C-25 was calculated to be 0.86. The ratio in paste AAS WG was 1.2. **Figure 7** shows the relationship between the compressive strength of pastes after 28 days of curing and the modules SiO_2/Na_2O in the activators where used glass wastes and reference waterglass. As it increases the modules SiO_2/Na_2O increases the mechanical strength [62].

Figure 6. ^{29}Si MAS NMR spectra for a) untreated solid glass waste; and b) liquid obtained after stirring waste in a $NaOH/Na_2CO_3$ solution for 2, 4 or 6 hours at 80 ± 2 °C

Figure 7. Relación entre resistencia a compresión a los 28 días de curado y el módulo de SiO_2/Na_2O de los activadores, con y sin residuos vítreos

The Hg porosimetry findings concurred with the data reported in the literature [63-65], according to which AAS mortars and concretes prepared with waterglass have lower total porosity values and greater microporosity than materials prepared with other activators, such as NaOH or $NaOH/Na_2CO_3$. The AAS N/C-25 pastes had total porosity and pore size distribution values closer to the values observed in paste AAS WG than in paste AAS N/C. BSEM/EDX microstructural analysis confirmed these differences in porosity (see **Figure 5**). There is a

relationship between porosity and compressive strength values that can be observed in **Figure 8**, whereas the curing time increases the total porosity decrease regardless of the type of solution used is produced [62]. This behavior is similar to Portland cement systems.

Figure 8. Relationship between the compressive strenths and the total porosity in AAS N/C, AAS WG and AAS N/C-25.

The characterisation techniques used in this study (FTIR and XRD) confirmed that the main reaction product in paste AAS N/C-25 was a C-A-S-H gel. Various calcium and calcium-sodium carbonates were identified in the pastes prepared with activators having Na_2CO_3 as a component.

Further to the present knowledge of the micro- and nanostructure of AAS pastes, the interaction between activating solution and vitreous slag yields C-A-S-H-type gels, whose composition and structure depend on the nature of the alkaline activator [46, 47]. When the activator is waterglass or similar, such as the activator prepared here with glass waste, the gel formed has a more condensed structure (longer mean chain length, more aluminium in its composition, more cross-linked or Q^3 units), which is the reason for the greater microporosity and consequently lower porosity and higher mechanical strength of these systems. In the present study, in terms of composition and structure, the C-A-S-H gel formed in paste AAS N/C-25 was observed to resemble the gel formed in paste AAS WG more closely than the gel in paste AAS N/C. The different SiO_2/Na_2O ratio in the AAS WG and AAS N/C-25 pastes explains the differences observed in the reactivity, structure and composition of the C-A-S-H gels formed (see **Tables 4** and **5**).

An analysis of the deconvoluted ^{29}Si and ^{27}Al MAS NMR spectra and the microstructural studies revealed structural and compositional differences among the calcium silicate hydrates formed with the three activators. These differences can be gleaned from **Table 6**, which gives data for the 7-day ^{29}SI MAS NMR spectra. The calcium aluminosilicate hydrate formed in paste AAS WG had a lower $Q^1/\Sigma Q^2$ ratio than the same product in the other two pastes. In other words, the former had a greater proportion of Q^2 units and consequently longer tetrahedral silicate chains (around 9 tetrahedra, see **Table 6**). Paste AAS WG also had a higher percentage of Q^3 units, denoting more intense inter-chain cross-linking and the formation of layered structures in some areas [47]. The ^{27}Al MAS NMR spectra, in turn, revealed a higher Al_T content in this gel.

More polymerised C-A-S-H gel structures have low Ca/Si ratios, such as obtained in this study (paste AAS WG had a Ca/Si ratio of around 0.9).

The mean chain lengths of the C-A-S-H gels, found with the Richardson method [52, 53, 58, 59] (**Table 6**), were shown to follow the pattern:

$$\text{AAS Wg} < \text{AAS N/C-25} < \text{AAS N/C}$$

The silicon present in the activator has been shown to contribute to the formation of calcium aluminosilicate hydrate in AAS WG paste [47, 48]. The findings for all the trials conducted here showed that the silicon present in glass waste (AAS N/C-25) also favoured the formation of a silicon-rich C-A-S-H gel. The ^{29}Si and ^{27}Al MAS NMR spectra confirmed greater reactivity in these pastes than in paste AAS N/C (from 73.34 % to 70.72 %, see **Table 6**), as well as more densely polymerised structures with higher $Q^1/\Sigma Q^2$ ratios, a larger proportion of Q^3-type cross-linked units and more Al_T in the gel structure, as deduced from smaller Ca/Si ratios (see **Table 5**).

Again, the differences between the AAS WG and AAS N/C-25 gel structure and composition were due to the difference in the activator SiO_2/Na_2O ratio.

Table 6. ^{29}Si and ^{27}Al MAS NMR parameters in activated pastes, by the activator used

5. Conclusions

The analytical finding showed in this work that silicon from glass waste dissolved in $NaOH/Na_2CO_3$ solutions can induce much the same effects as the silicon in waterglass, so these waste glasses can be used as activators in alkali activated systems (AAS).

The best conditions of solubility of these waste glasses were when we used a treatment with $NaOH/Na_2CO_3$ (pH=13.6) favoured the partial dissolution of the Si in the glass into its most reactive monomeric form.

The solutions resulting from the treatment of glass waste acted as alkaline activators, partially dissolving vitreous blast furnace slag and generating compounds and microstructures similar to the products observed in waterglass-prepared AAS. The behaviour of these pastes in terms of strength and microstructural development was comparable to the performance observed in AAS pastes prepared with conventional activators.

342 The present findings showed that the composition and structure of the C-A-S-H gels formed in
343 two AAS pastes, one prepared with waterglass and another with activators containing glass
344 waste, were similar. The differences observed between their reactivity, mechanical strength
345 and gel nano- and microstructure were due to the difference in the activator SiO_2/Na_2O ratios.

346

347 **6. Acknowledgements**

348 The present research was funded by the Ministry of Economy and Competitiveness under
349 project BIA2010-15516. The authors wish to thank P. Rivilla for her invaluable assistance with
350 the laboratory trials.

351 **References**

352 [1] L. Szabó, I. Hidalgo, J.C. Ciscar, A. Soria, CO_2 emission trading within the European Union
353 and Annex B countries: the cement industry case, Energy Policy 34 (2006) 72-87.

354 [2] N. Mahasenan, S. Smith, K. Humphreys, The Cement Industry and Global Climate Change:
355 Current and Potential Future Cement Industry CO_2 Emissions, in: Greenhouse Gas Control
356 Technologies-6th International Conference, Pergamon, Oxford (2003) 995-1000.

357 [3] A.O. Purdon, The action of alkalis on blast-furnace slag. J. Soc. Chem. Ind. 59 (1940) 191-
358 202.

359 [4] V.D. Glukhovsky, G.S. Rostovskaja, G.V. Rumyna, High strength slag-alkaline cements. 7th
360 International Congress Chem. Cem (Paris) 3 (1980) 164-168.

361 [5] V.D. Glukhovsky, Y. Zaitsev, V. Pakhomow, Slag-Alkaline cements and concretes-structures,
362 properties, technological and economic aspects of the use, Silic. Ind. 10 (1983) 197-200.

363 [6] J. Davidovits, Geopolymer chemistry and applications, Institut Geopolymere, Saint-Quentin
364 (2008) 3-12.

365 [7] C. Shi, X. Wu, M. Tang, Research on alkali-activated cemetitious systems in China: a review.
366 Adv. Cem. Res. 17 (5) (1993) 1-7.

367 [8] O.E. Gjorv, Alkali activation of a Norwegian granulated blast furnace slag. 3rd Intern. Conf.
368 Fly Ash, Silica Fume, Slag and Natural Pozzolans in Concrete, Trondheim, SPI114-73 (1989)
369 1501-1517.

370 [9] J. Mesto, The alkali reaction of alkali-activated finnish blast furnace slag. Silic. Ind. 47 (4-5)
371 (1982) 123-127.

372 [10] T. Kutti, Hydration products of alkali activated slag. 9th Intern. Congr. Chem. Cem. New
373 Delhi 4 (1992) 468-474.

374 [11] F. Puertas, Cementos de Escorias Activadas alcalinamente: Situación actual y perspectiva
375 de futuro, Mater. Construcc. 45 (239) (1995) 53-64.

376 [12] A. Fernández-Jiménez, J.G. Palomo, F. Puertas, Alkali-activated slag mortars: Mechanical
377 strength behaviour, Cem. Concr. Res. 29 (8) (1999) 1313-1321.

378 [13] F. Puertas, S. Martínez-Ramírez, S. Alonso, T. Vázquez, Alkali-activated fly ash/slag
379 cements. Strength behavior and hydration products, Cem. Concr. Res. 30 (10) (2000) 1625-
380 1632.

381 [14] A. Palomo, M.W. Grutzeck, M.T. Blanco, Alkali-Activated fly ashes a Cement for the future.
382 Cem. Concr. Res. 29 (1999) 1323-1329.

383 [15] A. Palomo, M.T. Blanco-Varela, M.L. Granizo, F. Puertas, T. Vázquez, M.W. Grutzeck,
384 Alkaline activation of metakaolin: Influence of synthesis Parameters. 10th Intern. Congrs.
385 Chem. Cem., Goteborg. (1997) Pp3ii 113.

386 [16] H. Xu, J.S.J. Van Deventer, The geopolymerisation of alumino-silicate minerals 59(3) (2000)
387 247-266.

388 [17] C. Shi, P. Krivenko, D. Roy, Alkali-activated cements and concretes, Taylor & Francis (2006)

389 [18] P. Duxson, A. Fernández-Jimenez, J.L. Provis, G.C. Luckey, A. Palomo, J.S.J. Deventer,
390 Geopolymer Technology: The current state of the art, J. Mater Sci 42(9) (2007) 2917-2933.
391
392 [19] C. Shi, A. Fernández-Jiménez, A. Palomo, New cements for the 21st century: The pursuit of
393 an alternatiave to Portland cement. Cem. Concr. Res. 41(7) (2011) 750-763.
394
395 [20] S.A. Bernal, R. Mejía de Gutiérrez, F. Ruiz, H. Quiñones, J.L. Provis, High-temperature
396 performance of mortars and concretes based on alkali-activated slag/metakaolin blends,
397 Mater. Construcc. 62, 308 (2012) 471-488.

398 [21] M. Palacios, P. Bowen, M. Kappl, H-J. Butt, M. Stuer, C. Pecharromán, U. Aschauer, F.
399 Puertas, Repulsion forces of superplasticizers on ground granulated blast furnace slag in

400 alkaline media, from AFM measurements to rheological properties, Mater. Construcc. 62, (308)
401 (2012) 489-513.

402 [22] J.L. Provis, Activating solution chemistry for geopolymers. In: Provis, J.L and van
403 Deventer, J.S.J (eds) Geopolymers: structures, processing, properties and Industrial
404 Applications, Woodhead, Cambrige, UK (2009) 50-71.

405 [23] M. Palacios, F. Puertas, Effect of shrinkage-reducing admixtures on the properties of alkali-
406 activated slag mortars and pastes. Cem. Concr. Res. 37 (5) (2007) 691-702.

407 [24] A. Fernández-Jiménez, A. Palomo, Composition and microstructure of alkali activated fly
408 ash binder: Effect of the activator, Cem. Concr. Res. 35 (2005) 1984-1992.

409 [25] G. Kovalchuk, A. Fernández-Jimenez, A. Palomo, Alkali-activated fly ash: Effect of termal
410 curing conditions on mechanical and microstructural development- Part II (Review), Fuel 86 (3)
411 (2007) 315-322.

412 [26] S.D. Wang, X.C. Pu, K.L. Scrivener, P.L. Pratt, Alkali-activated slag cement and concrete: a
413 review of properties and problems, Adv. Cem. Res. 7 (27) (1995) 93-102.

414 [27] K. Byfors, G. Klignstedt, V. Lehtonen, H. Pyy, L. Romben, Durability of concrete made with
415 alkali activated slag. 3rd Intern. Conf. Fly Ash, Silica fume, Slag and Natural Pozzolans in
416 concrete, Trondheim, SP 114-70 (1989) 1429-1466.

417 [28] S.D. Wang, K.L. Scrivener, Hydration products of alkali activated slag cement. Cem. Concr.
418 Res. 25 (3) (1995) 561-571.

419 [29] R. Mejía de Gutiérrez, J. Maldonado, C. Gutiérrez, Resistencia a temperaturas elevadas de
420 escorias activadas alcalinamente. Mater. Construcc. 54 (276) (2004) 87-92.

421 [30] A. Fernández-Jiménez, A. Palomo, Propiedades y aplicaciones de los cementos alcalinos.
422 Ing. Construcc. 24 (3) (2009) 213-232.

423 [31] A. Fernández-Jiménez, I. García-Lodeiro, A. Palomo, Durability of alkali-activated fly ash
424 cementitious materials. J. Mater Sci 42 (2007) 3055-3065.

425 [32] F. Puertas, R. de Gutiérrez, A. Fernández-Jiménez, S. Delvasto, J. Maldonado, Morteros de
426 cementos alcalinos. Resistencia química al ataque por sulfatos y al agua de mar. Mater.
427 Construcc. 52 (267) (2002) 55-71.

[33] J.M. Mejía, R. Mejía de Gutiérrez, F. Puertas, Rice husk ash as silica source in fly ash and ground blast furnace slag cementitious alkali activated systems. Mater. Construcc. 63 (311) (2013) 361-375.

[34] J. Larosa-Thomson, P. Gill, B.E. Scheetz, M.R. Silsbee, Sodium silicate applications for cement and concrete. Proc. 10th Int. Congr. On the Chemistry of Cement, Gothenburg, Vol.3.3 (1997).

[35] A.S. Brykov, V.I. Korneev, Production and usage of powdered alkali metal silicate hydrates. Metallurgist, Vol. 52 (2008) 11-12.

[36] M. Torres-Carrasco, J.G. Palomo, F. Puertas, Sodium silicate solutions from dissolution of glass wastes. Statistical analysis. Mater. Construcc. 64, 314 (2014). 10.3989/mc.2014.05213.

[37] M. Torres-Carrasco, F. Puertas, M.T. Blanco-Varela.: Preparación de cementos alcalinos a partir de residuos vítreos. Solubilidad de residuos vítreos en medios fuertemente básicos. XII Congreso Nacional de Materiales (Alicante) (2012).

[38] F. Puertas, M. Torres-Carrasco, C. Varga, J.J. Torres, E. Moreno, J.G. Palomo, Re-use of urban and industrial glass waste to prepare alkaline cements. 4th International Conference on Engineering for Waste and Biomass Valorization, Oporto (Portugal). (2012).

[39] J.M Fernández Navarro, El vidrio. Consejo Superior de Investigaciones Científicas. Sociedad Española de Cerámica y Vidrio. Madrid (2003).

[40] T.M. El-Shamy, J. Lewis, R.W. Douglas, The dependence on the pH of the descomposition of glasses by aqueous solutions. Glass Technology 13 (1972) 81-87.

[41] T.M. El-Shamy, C.G. Panteno, Descomposition of silicates glasses in alkaline solutions. Nature Vol. 266 (1977) 704-706.

[42] A. Paul, Chemical durability of glasses; a thermodynamic approach. J. Mater. Sci. 12 (1977) 2246-2268.

[43] K. Goto, J, States of silica in aqueous solution. II. Solubility of amorphous silica, Chem. Soc. Jap. Pure Chem Sect. 76 (1955) 1364-1366.

[44] F. Puertas, Torres, J.J, C. Varga, M. Torres-Carrasco, Spanish patent “Procedimiento para la fabricación de cementos alcalinos a partir de residuos vítreos urbanos e industriales”, PCT/ES2012/070408.

[45] R.D. Hooton, J.J. Emery, Glass content determination and strength development predictions for vitrified blast furnace slag. First Int. Conf. On the fly ash, silica fume, slag and other mineral by products in concrete. Montebello, Quebec, Canada, SP 79-SO (1983) 943-962.

[46] A. Fernández-Jiménez, F. Puertas, I. Sobrados, J. Sanz, Structure of Calcium Silicate Hydrates formed in Alkaline-Activated slag: Influence of the type of alkaline activator. J. Am. Ceram. Soc. 86 (8) (2003) 1389-1394.

[47] F. Puertas, M. Palacios, H. Manzano, J.S. Dolado, A. Rico, J. Rodríguez, A model for the C-A-S-H gel formed in alkali-activated slag cements. J. Eur. Cer. Soc. 31 (2011) 2043-2056.

[48] F. Puertas, A. Fernández-Jiménez, M.T. Blanco-Varela, Pore solution in alkali-activated slag cements pastes. Relation to the composition and structure of calcium silicate hydrate. Cem. Concr. Res. 34 (2004) 139-148.

[49] A. Fernández-Jiménez, F. Puertas, Setting of alkali-activated slag cement. Influence of activator nature, Adv. Cem. Res. 13 (3) (2001) 115-121.

[50] M. Palacios, F. Puertas, Effectiveness of Mixing time on hardened properties of waterglass-Activated slag pastes and mortars, Aci. Mater. Jour. 108 (1) (2011) 73-78.

[51] P.J. Schilling, L.G. Butler, A.Roy, H.C. Heaton, ^{29}Si and ^{27}Al MAS-NMR of NaOH activated blast-furnace slag. J. Am.Ceram. Soc. 77 (9) (1994) 2363-2368.

[52] I.G. Richardson, A.R. Brough, G.W. Groves, C.M. Dobson, The characterisation of hardened alkali-activated blast furnace-slag pastes and the nature of the Calcium Silicate Hydrate (C-S-H). Cem. Concr. Res. 24 (5) (1994) 813-829.

[53] I.G. Richardson, J.G. Cabrera, The nature of C-S-H in model slag-cements. Cem. Concr. Compos. 20 (2000) 259-266.

[54] G. Engelhardth, D. Michel, High Resolution Solid State NMR of Silicates and Zeolites. Wiley, Chichester, UK, (1987).

[55] I.G. Richardson, G.W. Groves, The structure of the calcium silicate hydrate phases present in the hardened pastes of white Portland cement/blast furnace slag blends. J. Mater. Sci 32 (1997) 4793-4802.

[56] P.J. Schilling, L.G. Butler, A.Roy, H.C. Heaton, ^{29}Si and ^{27}Al MAS-NMR of NaOH activated blast-furnace slag. J. Am. Ceram. Soc. 77 (9) (1994) 2363-2368.

[57] R.J. Kirkpatrick, X. Cong, An introduction to ^{27}Al and ^{29}Si NMR spectroscopy of cements and concretes. Application of NMR spectroscopy to cement science. Ed. P. Colombet and A. Grimmer (1994) 55-76.

[58] I. G. Richardson and G. W. Groves, The Incorporation of Minor and Trace Elements into Calcium Silicate Hydrate (C-S-H) Gel in Hardened Cement Pastes, Cem. Concr. Res. 23 (1993) 131-138.

[59] I. G. Richardson, The Nature of C-S-H in Hardened Cements, Cem. Concr. Res. 29 (1999) 1131-1147.

[60] M.A. Cincotto, A.A. Melo W.L. Repette, Effect of different activators type and dosages and relation to autogenous shrinkage of activated blast furnace slag cement. Proceedings of the 11th International Congress on the Chemistry of Cement. Durban (South Africa) (2003) 1878-1888.

[61] A. Fernández-Jiménez, F. Puertas, Effect of activator mix on the hydration and strength behavior of alkali-activated slag cements. Adv. Cem. Res. 15 (3) (2003) 129-136.

[62] S.D. Wang, K.L. Scrivener, P.L. Pratt, Factors affecting the strength of alkali-activated slag. Cem. Concr. Res. 24 (6) (1994) 1033-1043.

[63] F. Puertas, M. Palacios, T. Vázquez, Carbonation process of alkali-activated slag mortars, J. Mater. Sci. 41 (2006) 3071-3082.

[64] F. Colling, J.G. Sanjayan, Effect of pore size distribution on drying shrinkage of alkali-activated slag concrete, Cem. Concr. Res. 30 (9) (2000) 1401-1406.

[65] M. Palacios, F. Puertas, Effect of shrinkage-reducing admixtures on the properties of alkali-activated slag mortars, Cem. Concr. Res. 37 (5) (2007), 691-702.

[66] M. Criado, A. Fernández-Jiménez, A. Palomo, I. Sobrados, J.Sanz, Effect of the SiO_2/Na_2O ratio on the alkali activation of fly ash. Part II: ^{29}Si MAS-NMR Survey, Micropor. Mesopor. Mat. 109 (1-3) (2008) 525-534.

[67] A. Palomo, A. Fernández-Jiménez, M. Criado, Geopolímeros: una única base química y diferentes microestructuras, Mater. Construcc. 54 (275) (2004) 77-91.

Table 1. Chemical composition of slag and glass (wt %)

wt%	CaO	SiO_2	Al_2O_3	MgO	Fe_2O_3	S^{2-}	SO_3	Na_2O	K_2O	[1]L.O.I
Slag	41.00	35.54	13.65	4.11	0.39	1.91	0.06	0.01	-	2.72
Glass waste	11.75	70.71	2.05	1.17	0.52	-	-	11.71	1.08	0.83

[1]L.O.I = Lost on ignition

Table 2. SiO_2, Al_2O_3, CaO and MgO (g) from the glass waste dissolved after treatment in 100 ml of 50-per cent (wt) NaOH / Na_2CO_3

Glass waste	SiO_2 (g/ 100 ml)	Al_2O_3 (g/ 100 ml)	CaO (g/ 100 ml)	MgO (g/ 100 ml)
1 g	0.42	0.05	$1.2\ E^{-03}$	$1.5\ E^{-05}$
10 g	2.82	0.13	$5.3\ E^{-04}$	$3.0\ E^{-05}$
15 g	3.34	0.16	$6.1\ E^{-04}$	$4.3\ E^{-05}$
20 g	4.49	0.19	$6.9\ E^{-04}$	$7.2\ E^{-05}$
25 g	4.54	0.25	$8.2\ E^{-04}$	$2.0\ E^{-04}$

Table 3. Pastes prepared and activation conditions

Sample name	Activator type	L/S	Glass content	SiO_2/Na_2O	pH
***AAS N/C**	$NaOH/Na_2CO_3$	0.4	-	0	13.60
****AAS WG**	Waterglass	0.44	-	1.2	13.76
*****AAS N/C-1**	$NaOH/Na_2CO_3$	0.4	1 g	0.08	13.79
AAS N/C-10	$NaOH/Na_2CO_3$	0.4	10 g	0.54	13.70
AAS N/C-15	$NaOH/Na_2CO_3$	0.4	15 g	0.63	13.63
AAS N/C-20	$NaOH/Na_2CO_3$	0.4	20 g	0.85	13.60
AAS N/C-25	$NaOH/Na_2CO_3$	0.4	25 g	0.86	13.48

* AAS N/C = slag alkali activated with $NaOH/Na_2CO_3$
** AAS WG = slag alkali activated with waterglass
*** AAS N/C-(1-25) = slag alkali activated with $NaOH/Na_2CO_3$ and from 1 to 25 g of glass waste

Table 4. Deconvolution data for ^{29}Si and ^{27}Al MAS NMR spectra by the nature of the activator (anhydrous slag and 7-day pastes)

Sample		Q^0 (slag)	Q^0/Q^1 (slag)	Q^1 (end of chain)	Q^2 (1Al)	Q^2 (0Al)	Q^3 (1Al)	Q^3 (0Al)
Slag	Pos. (ppm)	-68.60	-75.50					
	Width	7.62	7.62					
	Integral (%)	20.54	79.46					
AAS N/C	Pos. (ppm)	-67.52	-73.40	-78.05	-81.90	-85.91	-91.07	-95.07
	Width	6.22	6.22	6.22	6.22	6.22	6.22	6.22
	Integral (%)	8.23	23.32	19.98	19.56	18.09	5.27	5.55
AAS WG	Pos. (ppm)	-66.92	-73.59	-78.47	-81.82	-85.86	-92.76	-97.47
	Width	7.05	7.05	7.05	7.05	7.05	7.05	7.05
	Integral (%)	6.26	20.08	15.69	18.05	27.80	7.41	4.71
AAS N/C-25	Pos. (ppm)	-66.59	-73.14	-78.17	-81.56	-85.50	-91.20	-96.30
	Width	6.65	6.65	6.65	6.65	6.65	6.65	6.65
	Integral (%)	6.22	23.06	19.25	18.10	23.30	5.59	4.48

Table 5. EDX determination of atomic radio

Sample	Zone	Number of analyses	Ca/Si	Al/Ca	Al/Si
AAS N/C	C-A-S-H gel	20	1.06 ± 0.07	0.35 ± 0.04	0.37 ± 0.05
AAS WG	C-A-S-H gel	20	0.80 ± 0.05	0.30 ± 0.03	0.24 ± 0.02
AAS N/C-25	C-A-S-H gel	20	0.94 ± 0.07	0.34 ± 0.04	0.31 ± 0.02

Table 6. ^{29}Si and ^{27}Al MAS NMR parameters in activated pastes, by the activator used

Parameters (%)	AAS N/C	AAS WG	AAS N/C-25
$^{\dagger}\alpha = Q^0 + Q_{slag}$	68.45	73.34	70.72
$^{\dagger\dagger}\Sigma Q^2/Q_{Total}$	0.55	0.62	0.58
Q^2 (0Al)/Q^2 (1Al)	0.92	1.54	1.28
$Q^1/\Sigma Q^2$	0.53	0.34	0.46
$\Sigma Q^3/Q^1 + \Sigma Q^2$	0.18	0.20	0.16
MCL (main chain length)	6.74	9.00	7.24

$^{\dagger}Q_{slag} = Q^0/Q^1$slag; $^{\dagger\dagger}Q_{Total} = \Sigma Q^n$ where Q^n stands for Q^1, Q^2 and Q^3 units

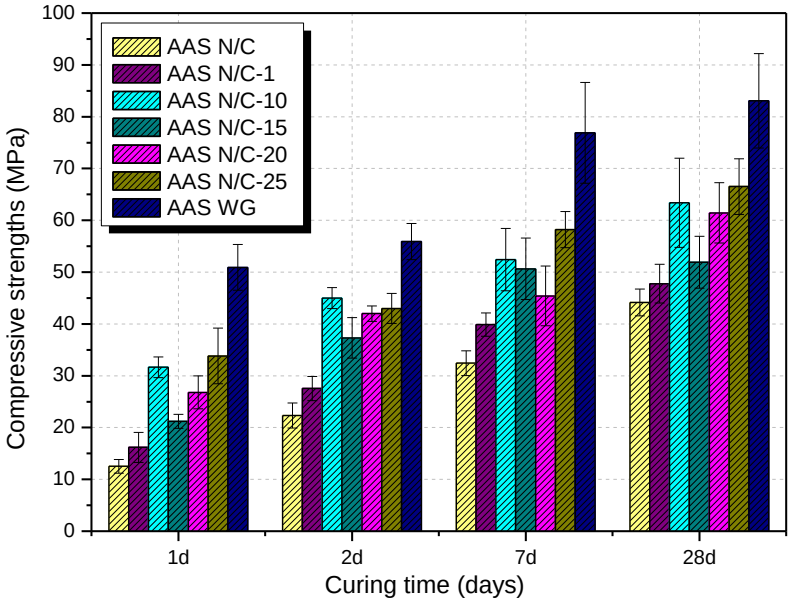

539

540 **Figure 1.** Compressive strength of AAS pastes prepared with different alkaline activators

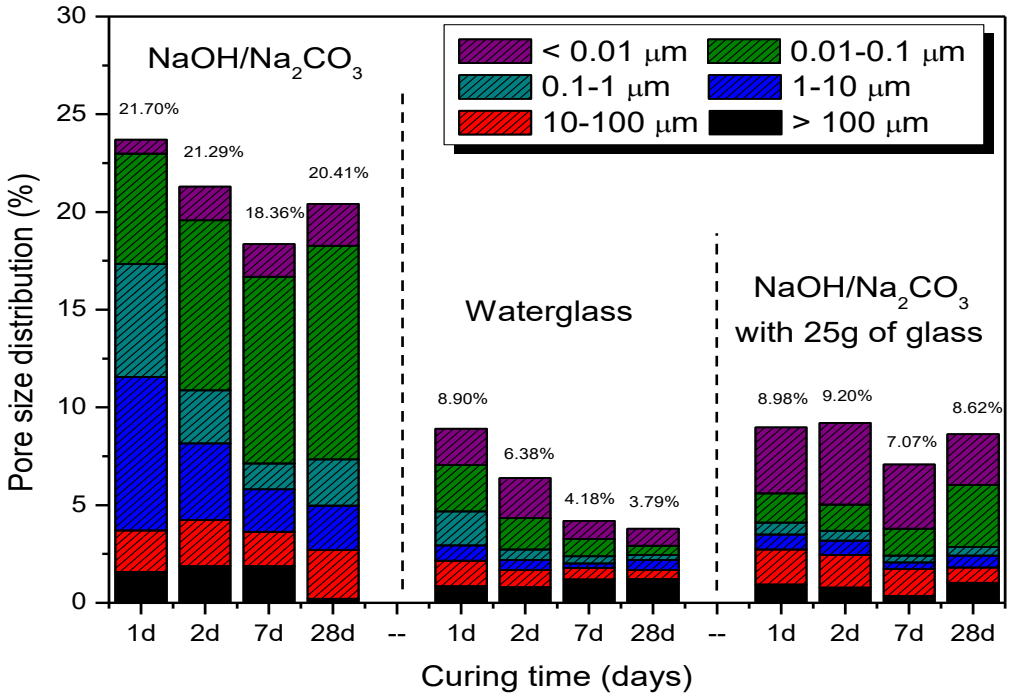

541

542 **Figure 2.** Pore size distribution in pastes AAS N/C, AAS WG and AAS N/C-25

543

544

545

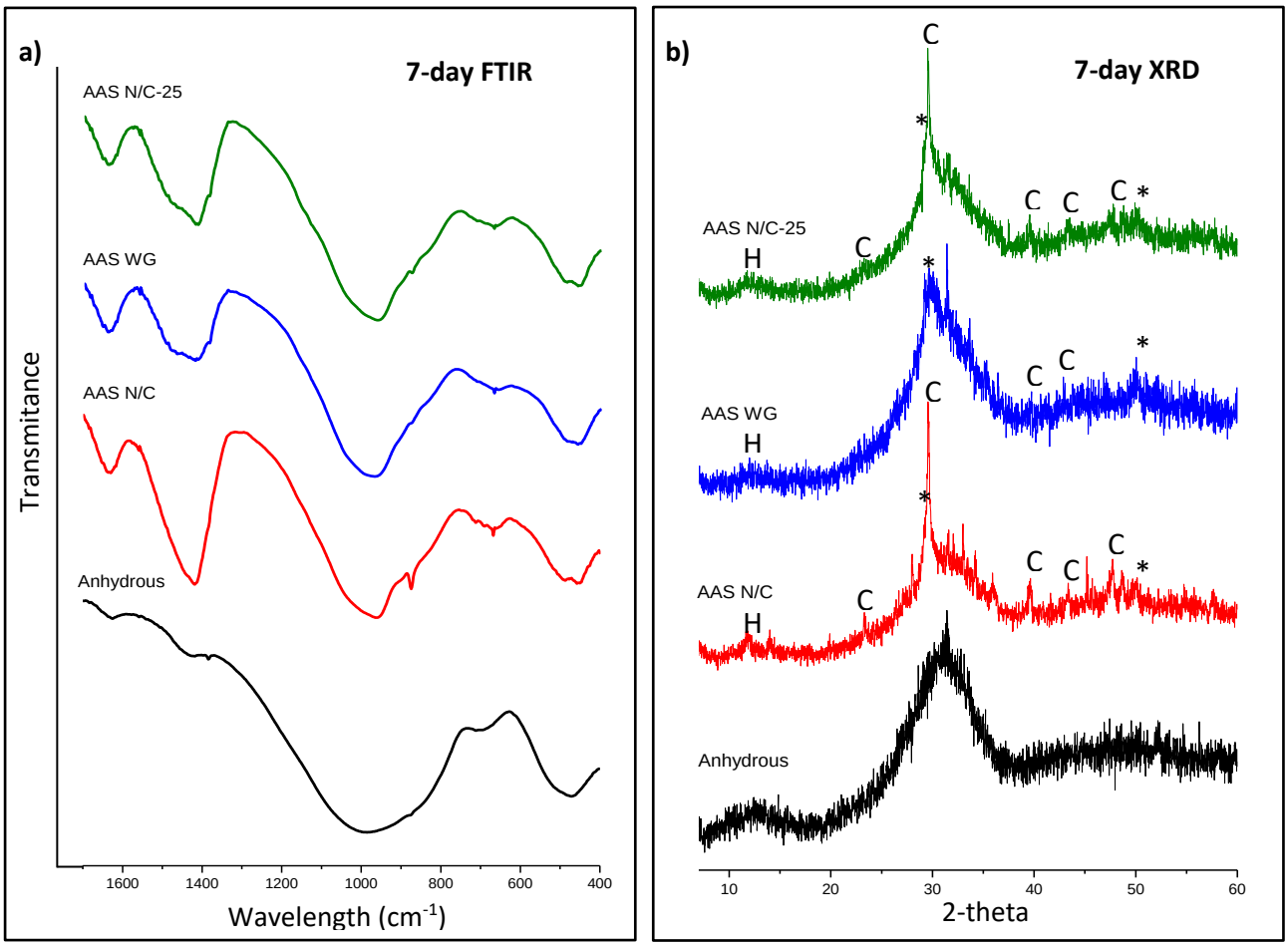

C = calcite, ***** = C-A-S-H gel, **H** = hydrotalcite

Figure 3. FTIR spectra for the anhydrous slag and 7-day pastes; b) XRD patterns for the anhydrous slag and 7-day pastes

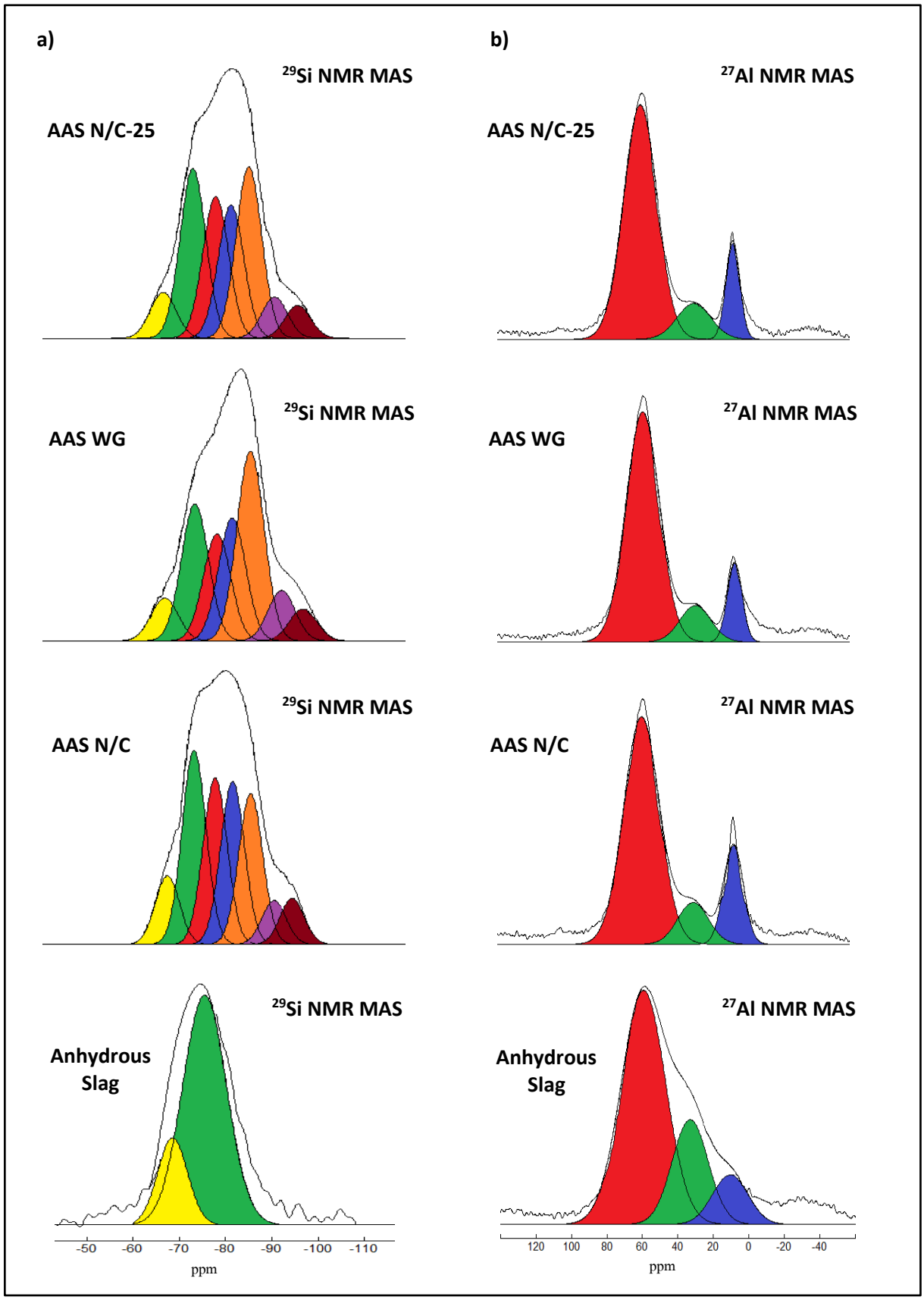

Figure 4. a) ^{29}Si and b) ^{27}Al MAS NMR spectra for the anhydrous slag and the 7-day alkali-activated pastes

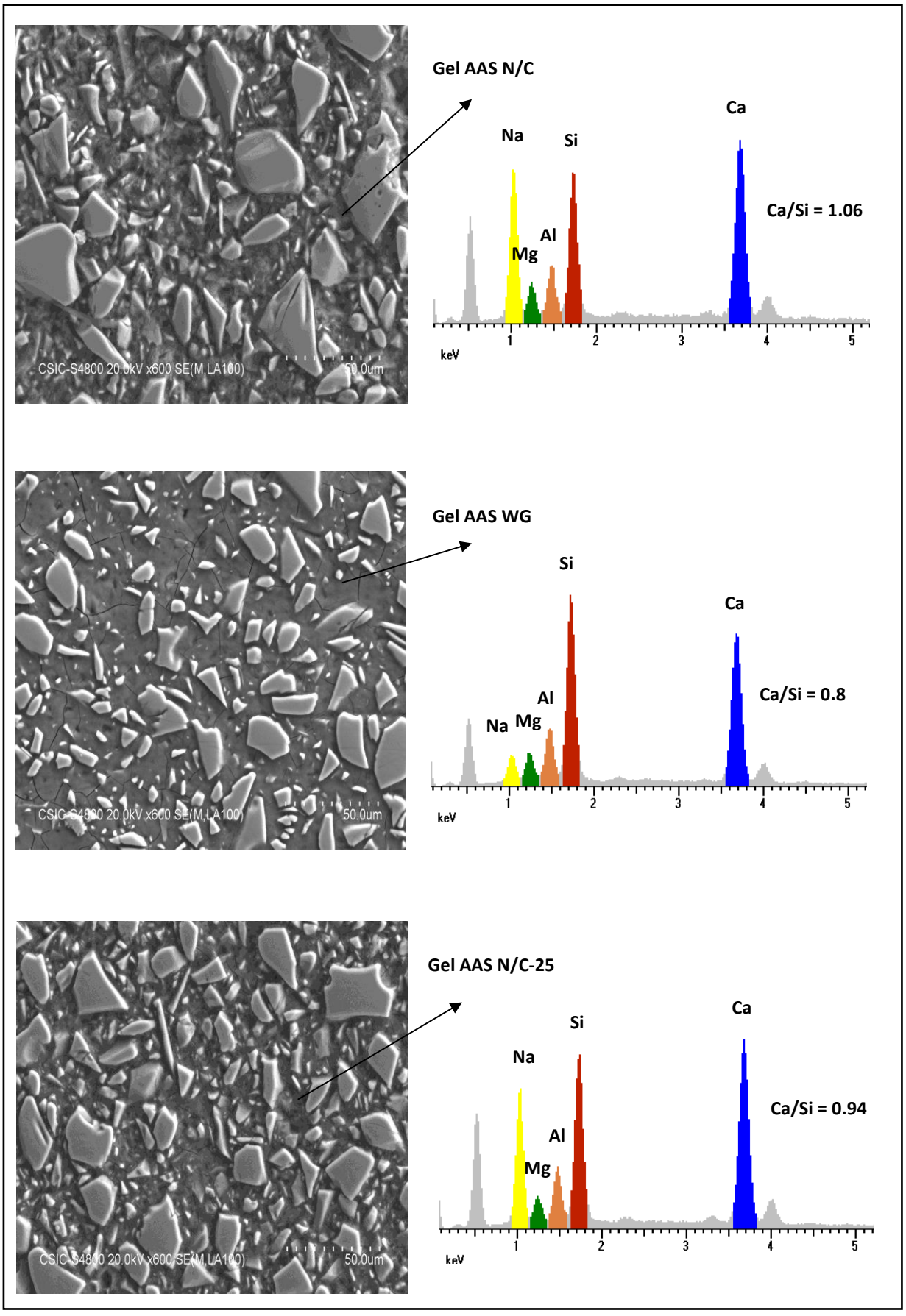

Figure 5. BSEM/EDX images of N/C-, WG- and N/C-25-activated slag pastes

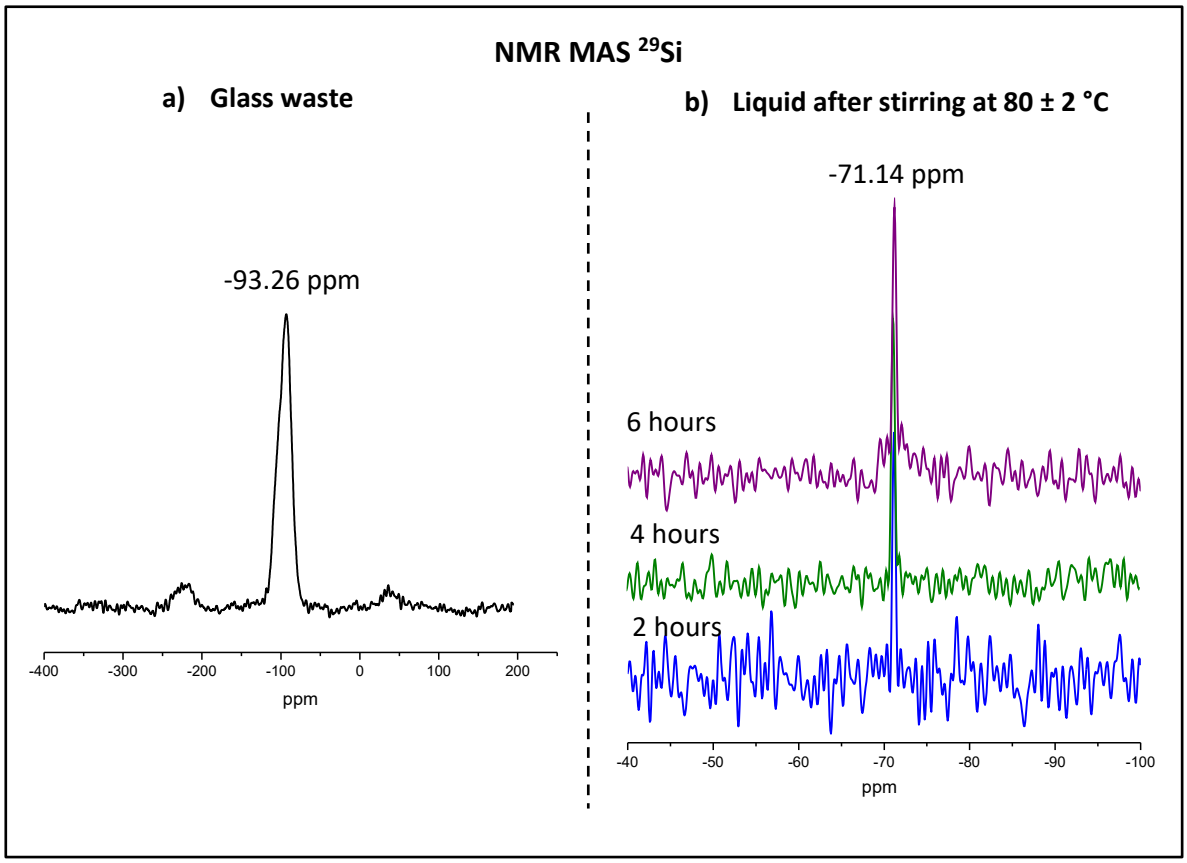

Figure 6. ^{29}Si MAS NMR spectra for a) untreated solid glass waste; and b) liquid obtained after stirring waste in a NaOH/Na_2CO_3 solution for 2, 4 or 6 hours at 80 ± 2 °C

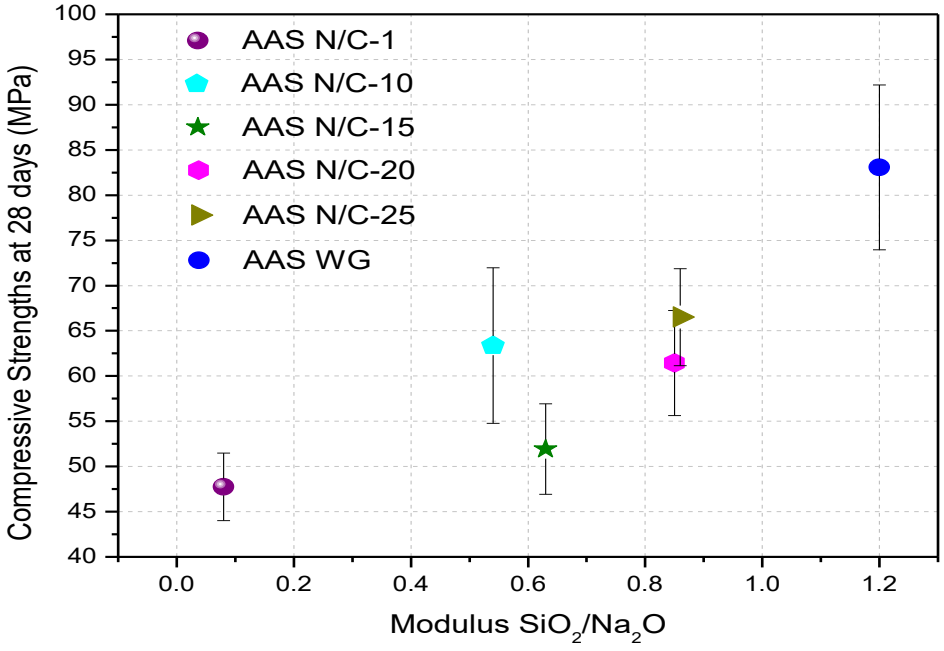

Figure 7. Relación entre resistencia a compresión a los 28 días de curado y el módulo de SiO_2/Na_2O de los activadores, con y sin residuos vítreos

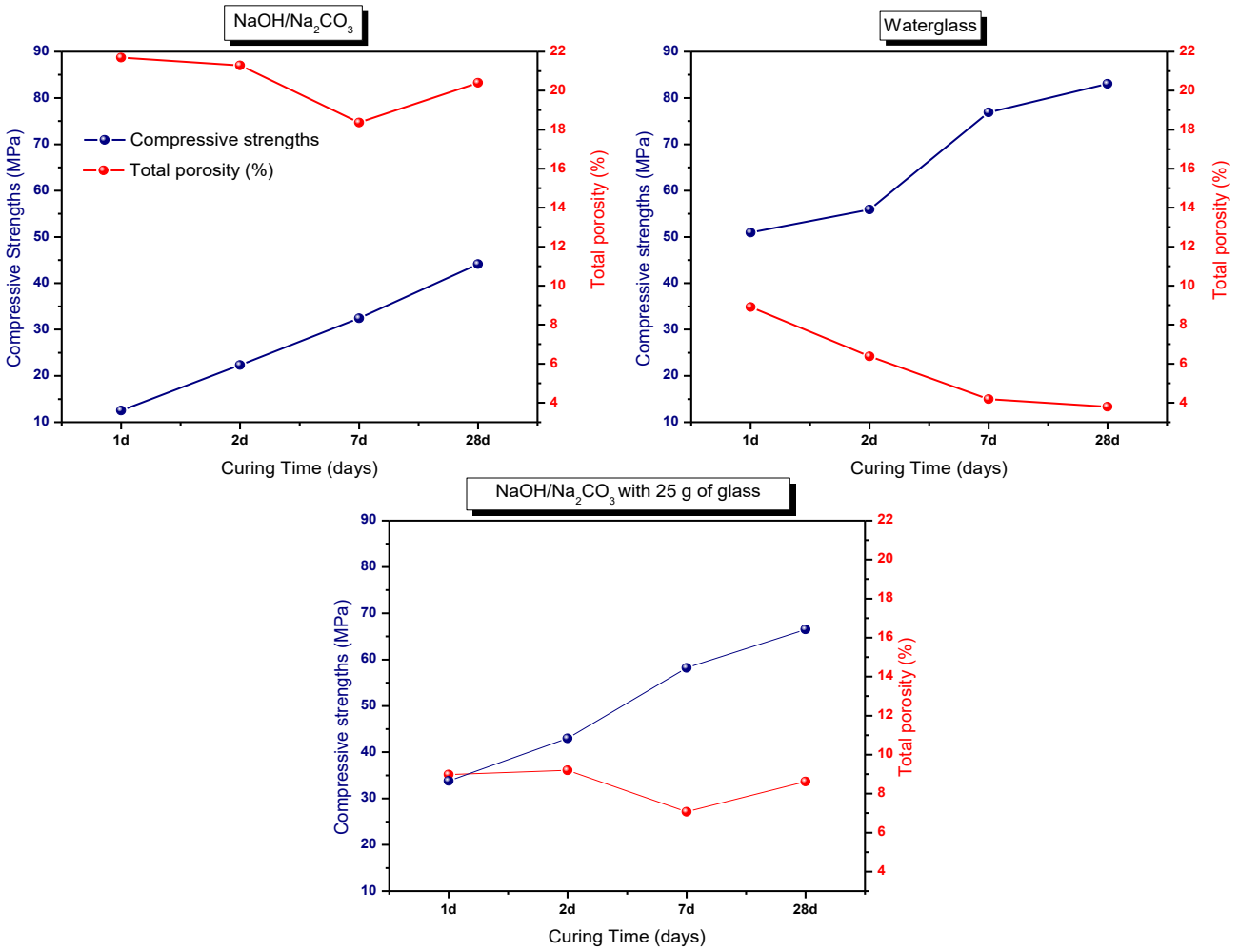

646

647 **Figure 8.** Relationship between the compressive strengths and the total porosity in AAS N/C,

648 AAS WG and AAS N/C-25.

649